ECCOMAS Congress 2016
VII European Congress on Computational Methods in Applied Sciences and Engineering
M. Papadrakakis, V. Papadopoulos, G. Stefanou, V. Plevris (eds.)
Crete Island, Greece, 5–10 June 2016

REINFORCEMENT CORROSION IN CONCRETE DUE TO CARBONATION AND CHLORIDE INGRESS UP AND BEYOND INDUCTION PERIOD

K. Hájková[1], L. Jendele[2], V. Šmilauer[1], T. Sajdlová[2], J. Červenka[2]

[1] Czech Technical University in Prague, Faculty of Civil Engineering
Thákurova 7; 166 29, Prague 6; CZ
e-mail: {karolina.hajkova, vit.smilauer}@fsv.cvut.cz

[2] Červenka Consulting s.r.o.
Na Hřebenkách 55, 150 00, Prague, CZ
{libor.jendele, tereza.sajdlova, jan.cervenka}@cervenka.cz

Keywords: Concrete, corrosion, propagation phase, carbonation, chloride ingress

Abstract. *Carbonation and chloride ingress are considered to be the most severe mechanisms for steel corrosion in reinforced concrete structures. Here, the service life is traditionally divided into two main phases; the initial and the propagation ones. The initial phase was explored recently and the results show high influence of cracks on accelerating of carbonation and chloride ingress in concrete structures. Our model focuses now on the propagation period and predicts x_{corr} for radial corrosion depth, including cracking and spalling of concrete cover. The presented models were implemented in ATENA software and demonstrate their application on a prestressed box-girder bridge. The simulation shows reinforcement corrosion due to carbonation and chloride ingress, and its impact on a bridge behavior during ULS analysis.*

1 INTRODUCTION

Reinforcement corrosion due to carbonation and chloride ingress are the most damaging mechanisms in reinforced concrete structures. The service life t_l of reinforced concrete structures is generally divided into two time phases; the initiation (induction) period t_i and the propagation period t_p. The initiation period for damaging mechanisms was described and validated in the previous paper [1] and preliminary results show strong influence of cracks to transport properties and acceleration of damaging mechanisms. For traditional cement-based materials, cracks 0.3 mm decrease induction time approximately 6 times for carbonation and approximately 9 times for chloride ingress of sea water. Preventing macrocracks and designing proper concrete is essential for durable concrete [1].

Our model focuses on the propagation period t_p where corrosion of reinforcing steel takes place. During this period, reinforcement decreases and accompanied with growing corrosion products. Corrosion of reinforcement is described according to the general diagram in Figure 1. A uniform corrosion (the most widespread form of corrosion) is characteristic for carbonation and a pitting corrosion (creation of small pits) for chlorides [2]. The cracking of concrete cover during propagation period $t_{p,cr}$ corresponds to the depth of corrosion $x_{corr,cr}$ and spalling of concrete cover $t_{p,sp}$ corresponds to the depth of penetration $x_{corr,sp}$ [3].

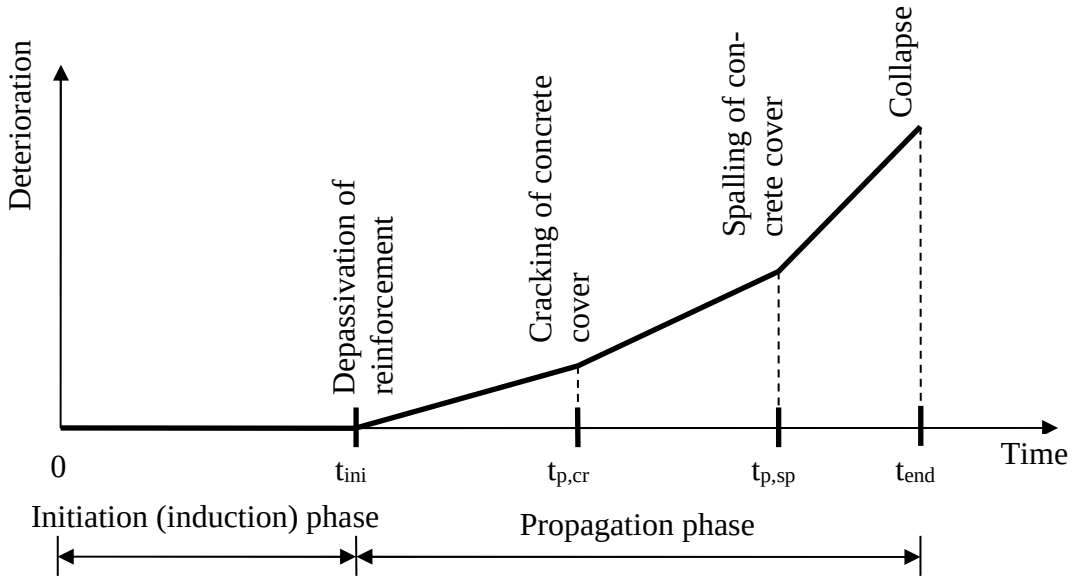

Figure 1: Initiation and propagation phase [3]

2 MODELS FOR PROPAGATION PHASE

2.1 Carbonation during propagation phase

The corrosion rate for the carbonation depends on the corrosion current density i_{corr} [$\mu A/cm^2$], which ranges between 0.1-10 (passive corrosion-high corrosion) and depends on the quality and the relative humidity of the concrete [5]. This model predicts amount of corroded steel during the whole propagation period t_p. The corrosion rate is based on Faraday's law [4], determined as follows:

$$\dot{x}_{\mathrm{corr}}(t) = 0.0116 i_{\mathrm{corr}}(t) \tag{1}$$

where $\dot{x}_{\text{corr}}$ is the average corrosion rate in the radial direction [μm/year], i_{corr} is corrosion current density [μA/cm^2] and t is calculated time after the end of induction period [years].

By integration of Eq. (1), it is obtained the corroded depth for 1D propagation:

$$x_{\text{corr}}(t) = \int_{t_{ini}}^{t} 0.0116 i_{\text{corr}}(t) R_{\text{corr}} \, \mathrm{d}t \tag{2}$$

where x_{corr} is the total amount of corroded steel in radial direction [mm] and R_{corr} is parameter, depends on the type of corrosion [-]. For uniform corrosion (carbonation) $R_{corr} = 1$, for pitting corrosion (chlorides) $R_{corr} = <2; 4>$ according to [9] or $R_{corr} = <4; 5.5>$ according to [10].

Effective bar diameter for both types of corrosion is obtained from:

$$d(t) = d_{ini} - \psi 2 x_{corr}(t) \tag{3}$$

where $d(t)$ is evolution of bar diameter in time t, d_{ini} is initial bar diameter [mm], ψ is uncertainty factor of the model [-], mean value $\psi = 1$ and x_{corr} is the total amount of corroded steel according to (2).

2.2 Chloride ingress during propagation phase

The corrosion rate for chlorides is more complicated because it is affected by concentration of chlorides in the concrete. Calculation of corrosion current density was formulated by Liu and Weyer's model [6]:

$$i_{corr} = 0.926 \cdot \exp\left[7.98 + 0.7771 \ln(1.69 C_t) - \frac{3006}{T} - 0.000116 R_C + 2.24 t^{-0.215} \right] \tag{4}$$

where i_{corr} is corrosion current density [μA/cm^2], C_t is total chloride content [kg/m^3 of concrete] on reinforcement which is determined from 1D nonstationary transport, T is temperature at the depth of reinforcement [K] and R_c is ohmic resistance of the cover concrete [Ω] [7] and t is time after initiation [years]:

$$R_C = \exp[8.03 - 0.549 \ln(1 + 1.69 C_t)] \tag{5}$$

The average corrosion rate in radial direction is determined further when plugging (6),(7) to (1). The total amount of corroded steel in radial direction stems from (2) and the effective bar diameter from (3).

2.3 Cracking of concrete cover

Cracking of concrete cover for both carbonation and chlorides can be estimated from DuraCrete model which provides realistic results [3]. The critical penetration depth of corroded steel $x_{corr,cr}$ is formulated as:

$$x_{corr,cr} = a_1 + a_2 \frac{C}{d_{ini}} + a_3 f_{t,ch} \tag{8}$$

where parameter a_1 is equal 7.44e-5 [m], parameter a_2 is equal 7.30e-6 [m], a_3 is [-1.74e-5 m/MPa], C is cover thickness of concrete [m], d_{ini} initial bar diameter [m], $f_{t,ch}$ is characteristic splitting tensile strength of concrete [MPa].

2.4 Spalling of concrete cover

The critical penetration depth of corroded steel $x_{corr,sp}$ for both carbonation and chlorides is calculated from [3] as:

$$x_{corr,sp} = \frac{w^d - w_0}{b} + x_{corr,cr} \tag{9}$$

where parameter b depends on the position of the bar (for top reinforcement 8.6 µm/µm and bottom 10.4 µm/ µm), w^d is critical crack width for spalling (characteristic value 1 mm), w_0 is width of initial crack (known from previous ATENA computation) and $x_{corr,cr}$ depth of corroded steel at the time of cracking [m].

After spalling of concrete cover, corrosion of reinforcement takes place in direct contact with the environment. To determine the rate of corrosion of reinforcement after spalling, Table 1 gives rates of reinforcement corrosion [8].

Corrosivity zone (ISO 9223)		Typical environment	Corrosion rate for first year (µm/y)	
Category	Description		Mild steel	Zinc
C1	Very low	Dry indoors	≤1,3	≤0,1
C2	Low	Arid/Urban inland	>1,3 a ≤25	>0,1 a ≤0,7
C3	Medium	Coastal and industrial	>25 a ≤50	>0,7 a ≤2,1
C4	High	Calm sea-shore	>50 a ≤80	>2,1 a ≤4,2
C5	Very High	Surf sea-shore	>80 a ≤200	>4,2 a ≤8,4
CX	Extreme	Ocean/Off-shore	>200 a ≤700	>8,4 a ≤25

Table 1: Corrosion rates of steel under atmospheric exposition

3 ANALYSIS OF A PRESTRESSED CONCRETE BRIDGE

The present model can be used for a wide range of structures from civil engineering. This is documented on an assessment of a prestressed box-girder concrete bridge of Mr. Pavel Wonka over the river Elbe in Pardubice, Czech Republic. It is beyond the scope of this paper to present detailed results from this analysis and hence, only the most important global results and results related to the presented durability analysis of the bridge are given. More details are available in [12], including material parameters, description of the bridge geometry and prestressing tendons etc.

The bridge was designed and erected between 1956 and 1959. The structure is depicted in Figure 2. The bridge consists of three arches, having spans 50 + 70 + 50 m. Average depth of cross sections is up to 3.5 m.

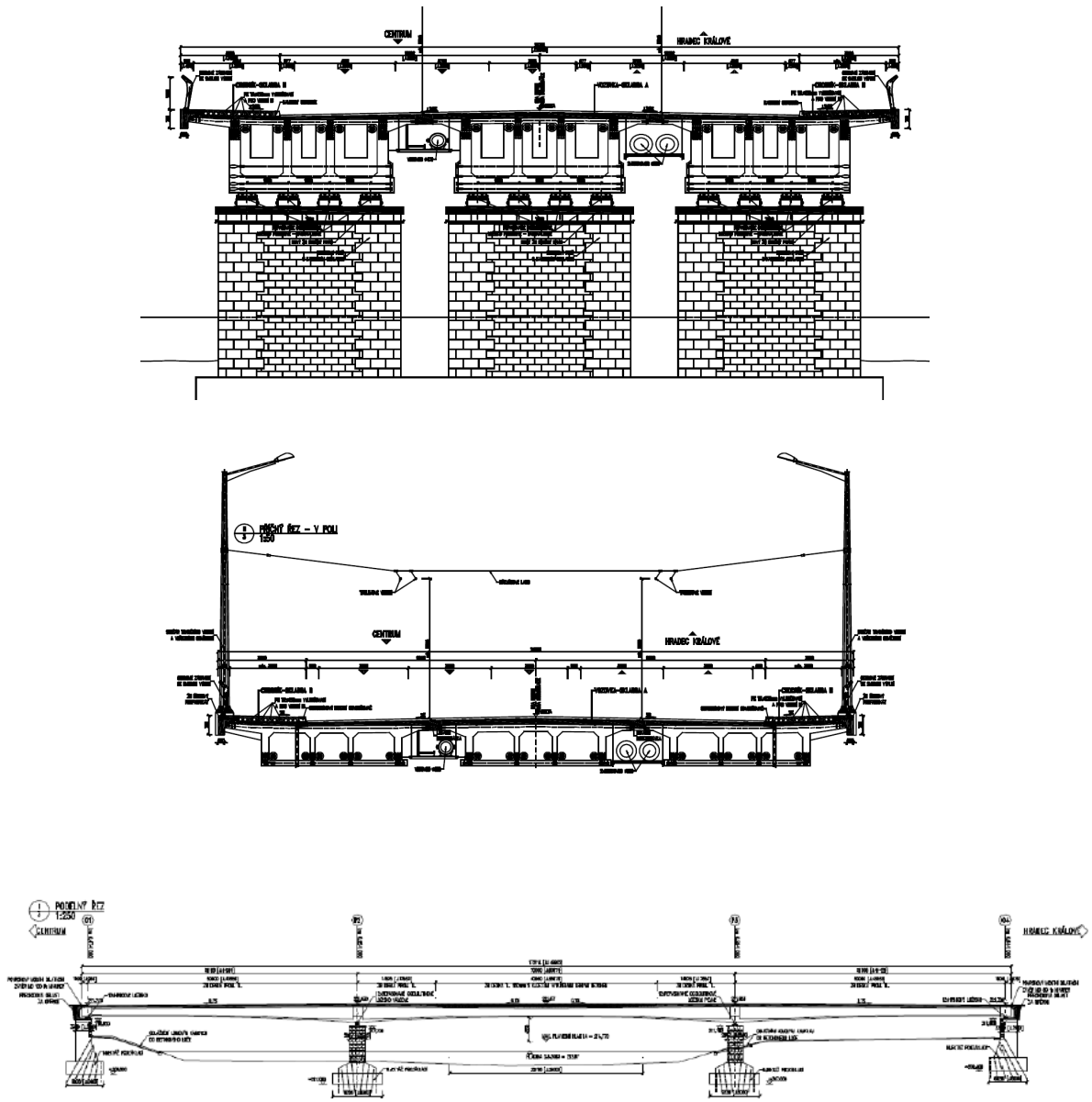

Figure 2: Dimensions of the bridge: drawing of cross section near the pillars, (top picture), mid-span cross section, (middle picture), and side (longitudinal) view of the bridge, (bottom picture) [11]

The structure was analyzed by program ATENA with implemented durability models [11]. The bridge is modeled by 4512 layered shell elements. The structure near supports and some other details are modeled by hexahedral and wedge solid elements. The pre-stressed tendons are realized by 3022 external cable truss elements, while the conventional reinforcement is introduced by embedded reinforcement within shell elements. A special material model for concrete and tendons has been employed with more details in [12].

The analysis of the bridge consists of three parts. The first analysis replicates in-situ load tests and measurements. The bridge was loaded by its self-weight and by tens of loaded trucks simulating a traffic load. It was used to calibrate the model of the bridge.

In the second part, numerical model was used to investigate service load state (SLS) and ultimate load state (ULS) of the bridge. Applied steps of the analysis and the associated loads were as follows:

1. Self-weight of the load-bearing structure and pre-stressing, (steps 1...10)
2. Weight of the top layers of the bridge, i.e. road etc., (steps 11...15)
3. Extra 35% of the load in the item 2, (steps 16...20)
4. 150% of the traffic load of the bridges according to ULS ČSN EN 1991-2, (steps 21...27)
5. Additional extra load according to the item 4. incremented up to failure of the bridge, (steps 28...78)

Deformation of the bridge at the 10th step and crack development at one end of the bridge is depicted in Figure 3 and Figure 4.

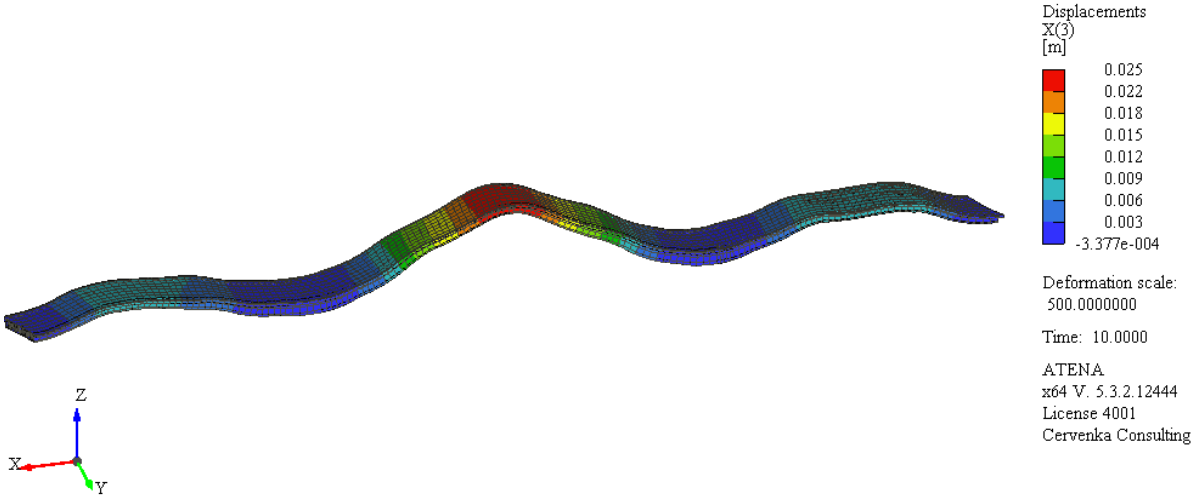

Figure 3: Deformation of the bridge at step 10, i.e. after self-weight and pre-stressing, (enlarged 500x)

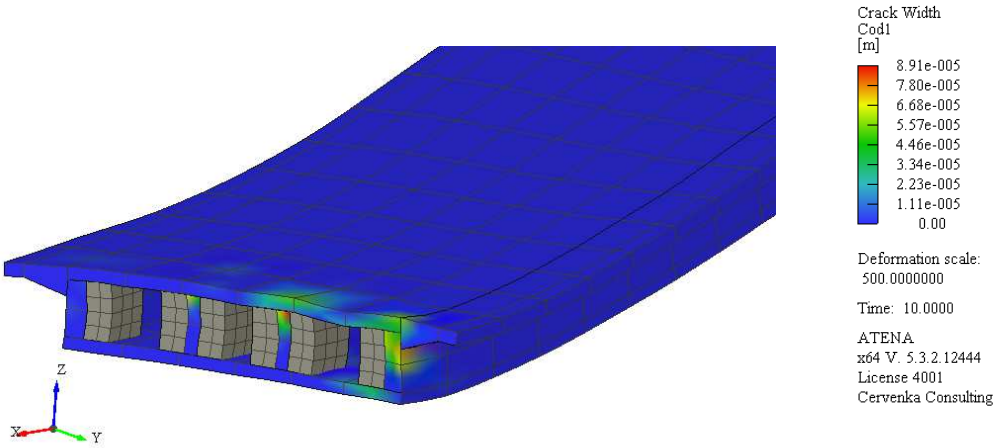

Figure 4: Crack development at the abutment of the bridge

Deformation of the bridge near its failure is shown further in Figure 5. It occurred at about 130% of the design load of the bridge, (i.e. steps 1...27 during loads 1-4). Load displacement diagram of the ULS analysis for centre of the central arch of the bridge is shown in Figure **6**, including prestress transfer.

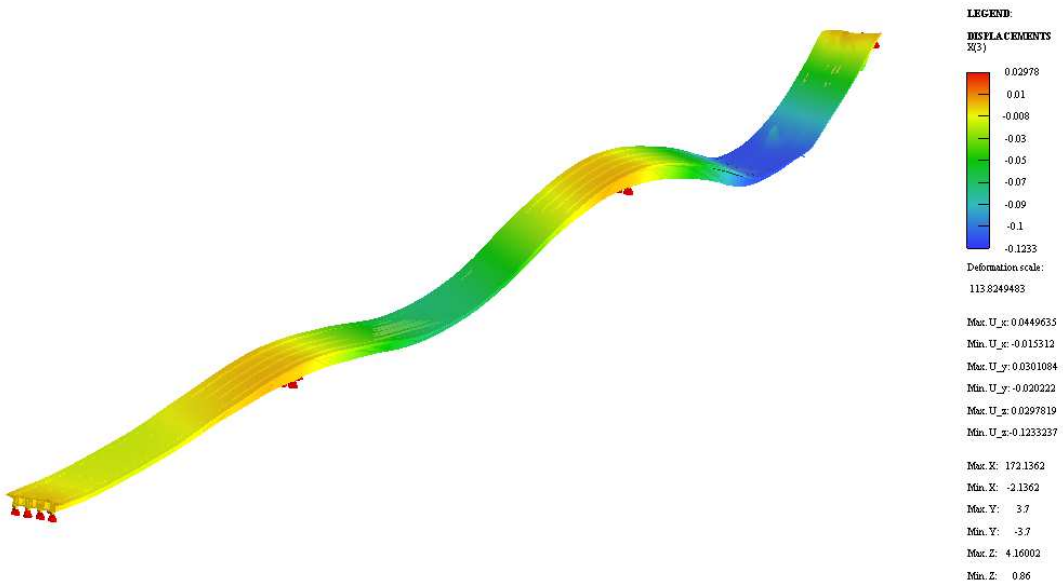

Figure 5: Deformation near failure of the bridge

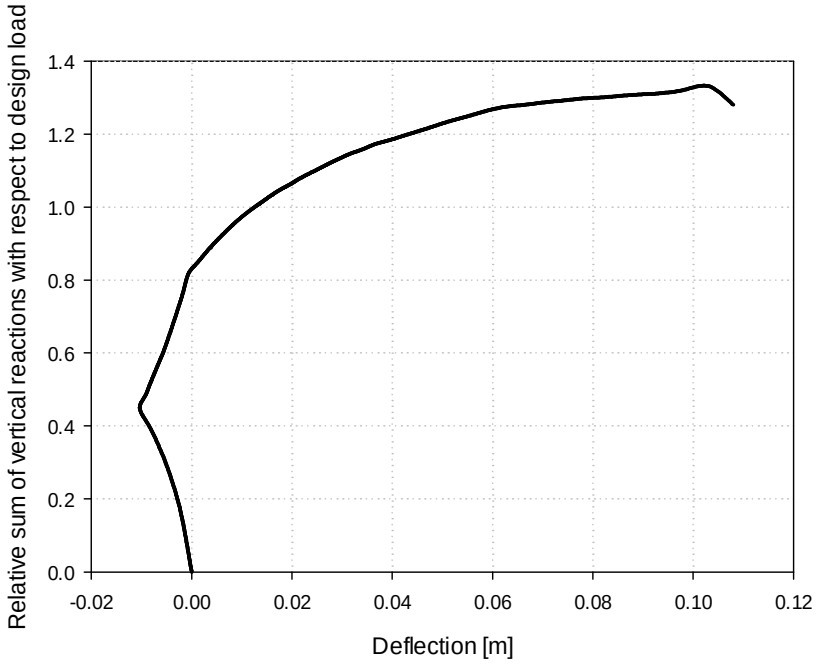

Figure 6: Load-displacement diagram of the ULS analysis - center of the central arch.

The third part of the analysis is devoted for durability study. According to direct concrete testing in 2003, concrete of the box-girder was classified as C35/45. An estimated composition yields CEM 42.5 350 kg/m^3 and water content 175 kg/m^3.

Concrete box-girder was loaded on its surface by carbonation and chlorides as described below. This analysis restarted from the step 27, (i.e. from the level of design load) and carbonation and chlorides load was applied for another 150 years simultaneously. The chlorides and carbonation loads used the following parameters:

- Carbonation: C_p = 350 kg/m^3, SCM = 0, W = 175 kg/m^3, CO_2 = 0.00036, RH = 0.60. Progressive period a_1 = 7.44e-5 m, a_2 = 7.30e-6 m, a_3 = -1.74e-5 m/MPa, $f_{t,ch}$ =

3.5 MPa, d_{ini} = 0.001 m, pitting corrosion R_{corr} =1, corrosion rate after spalling 30 μm/year.

- Chlorides: D_{ref} = 1.19e-7 m^2/day (mean value would be D_{ref} = 7.72e-13·86400 = 6.67e-08 m^2/day), t_{Dref} = 3650 days, m_{coeff} = 0.37, t_{mcoeff} = 10950 days, C_s = 0.103, Cl_{crit} = 0.0185. Progressive period a_1 = 7.44e-5 m, a_2 = 7.30e-6 m, a_3 = -1.74e-5 m/MPa, $f_{t,ch}$ = 3.5 MPa, w_d = 0.001 m, pitting corrosion R_{corr} = 3, corrosion rate after spalling 30 μm/year.

Chloride ingress assumed concentration of sea water on the surface; this resembles situation when salt brine water had leaked through insulation and the Cl concentration rose up substantially. According to Duracrete [3], spray zone from de-icing salts identified a slightly lower concentration C_s = 0.0776. Also, 90% confidence was considered for diffusivity D_{ref}, which is about twice higher than the mean value for this concrete strength class.

Figure **7** brings plot of maximum vertical displacement of the bridge vs. age of the structure. Note that the significant increase of the deflection at later times is due to tendons corrosion only as creep is neglected in computation and the force load is kept constant.

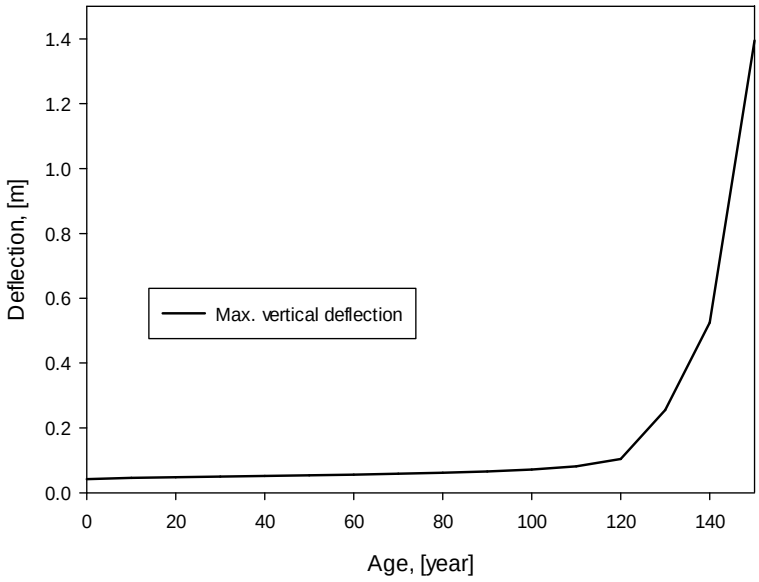

Figure 7 Maximum deflection of the bridge due to tendons corrosion

Figure 8 shows that carbonation depth is 58 mm for 150 years on uncracked concrete. Induction period for chlorides is much shorter, approximately 15 years with uncracked concrete cover 55 mm.

As far as steel corrosion is concerned, Figure 9 depicts calculated reduction coefficient for a pre-stressing tendon with concrete cover 55 mm. Reduction coefficient 1 means no corrosion, while value 0 signalizes total loss. For the first 12 years, the reinforcement does not corrode at all. Corrosion due to chlorides starts at 12 years. Corrosion due to carbonation begins after 110 years. At the age of 100 years about 60% of the reinforcement has corroded and at 150 years there is only about 35% of the original reinforcement. As expected, the effect of chlorides is much more devastating than that of carbonation. This is also documented by Fig-

ure 10, which shows total reinforcement reduction factor for the pre-stressing tendons at age of 150 years.

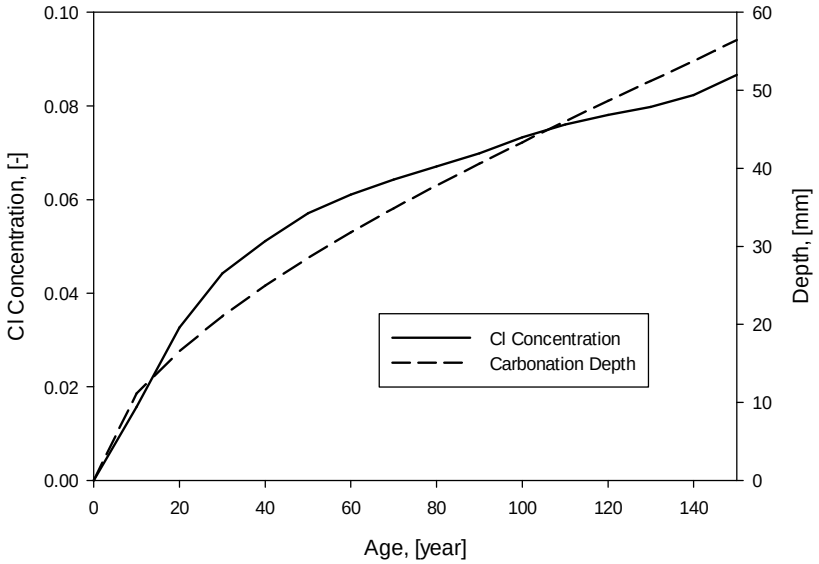

Figure 8: Characteristic carbonation depth for uncracked concrete. Chloride concentration for uncracked concrete at 55 mm from exposed surface

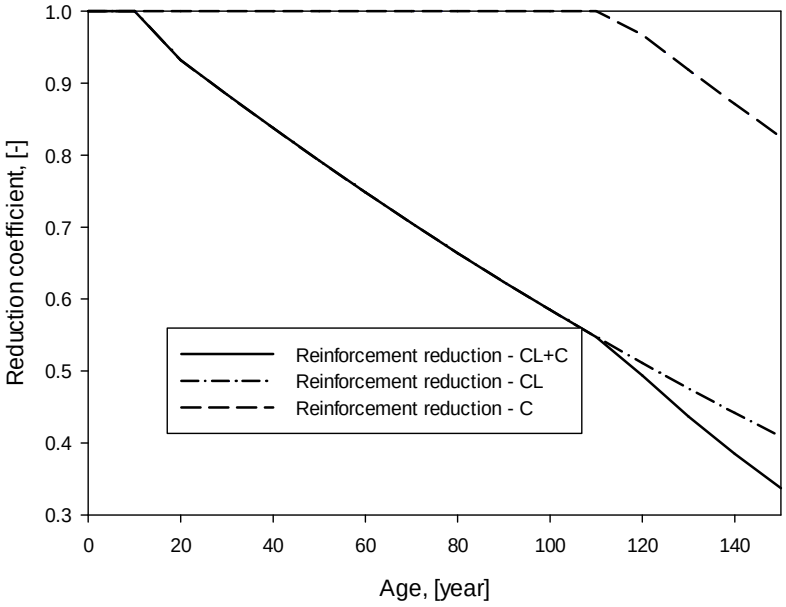

Figure 9 Computed reduction coefficient for a tendon, concrete cover 55 mm with the influence of cracks

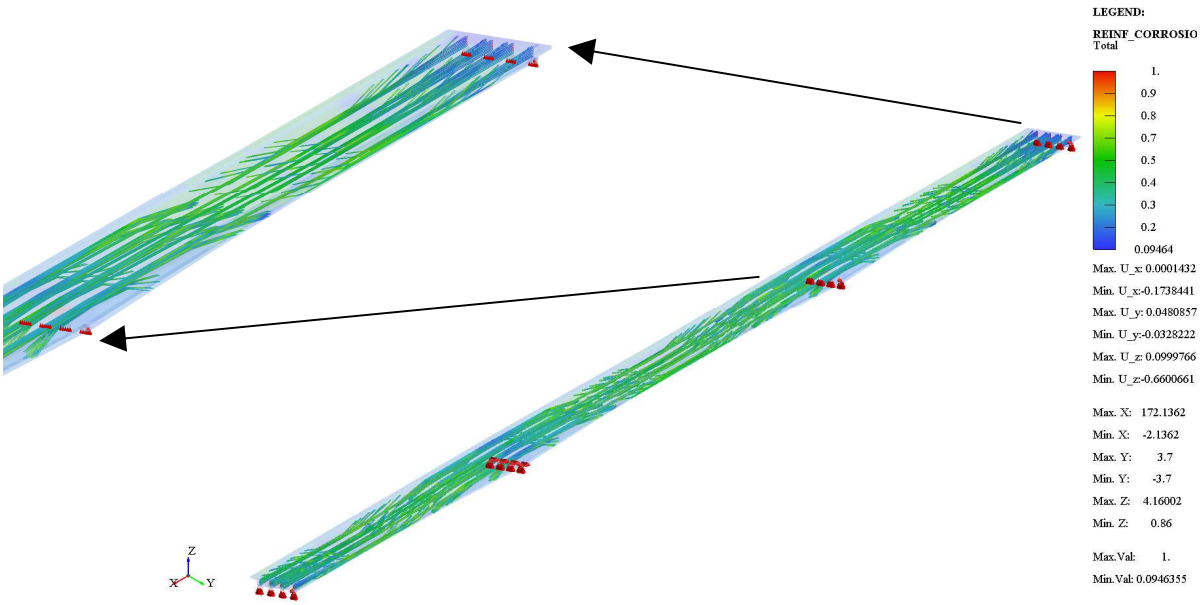

Figure 10: Total reduction coefficients for tendons at 150 years

4 CONCLUSIONS

The implemented durability model for reinforcement corrosion due to carbonation and chloride ingress focused on the propagation period where corrosion of reinforcement and spalling take place.

- The presented models provide induction time and reduction of tendons during the propagation period. The collapse of the bridge can be predicted when combined with ULS analysis.
- Results for a prestressed box-girder bridge indicate that tendon corrosion would start at 12 years if high external chloride concentration is assumed. At 100 years, about 60% of tendons' cross section remains and at 150 years this drops to only 30%.
- Durability analysis could be an integral part of bridge assessment, using slightly extended model. It allows prediction of negative effects of external environmental conditions on the structure and exploring deterioration.

Acknowledgement: We gratefully acknowledge the financial support from the Technology Agency of the Czech Republic TAČR under the project TA04031458 and SGS12/116/OHK1/2T/11 granted by Czech Technical University in Prague.

REFERENCES

[1] V. Šmilauer, L. Jendele, J. Červenka, Prediction of Carbonation and Chloride Ingress in Cracked Concrete Structures, *International conference on civil structural and environmental engineering computing*, 2013.

[2] F. Duprat, Reliability of RC Beams Under Chloride-ingress. *Construction and Building Materials*, **21**, 1605-1616, 2007.

[3] DuraCrete, Final Technical Report, 2000.

[4] J. Rodriguez, L. M. Ortega, J. Casal & J. M. Diez, Corrosion of Reinforcement and Service Life of Concrete Structures. In Proc. of Int. Conf. on Durability of Building Materials and Components, 7, Stockholm, 1:117-126, 1996.

[5] Page CL, Nature and properties of concrete in relation to environment corrosion, *Corrosion of Steel in Concrete*, Aachen, 1992.

[6] Liu Y, Weyers R.E., Modeling the Dynamic Corrosion Process in Chloride Contaminated Concrete Structures, *Cement and Concrete Research*, **28**(3), 365-367, 1998.

[7] Liu Y., Modelling the Time-to-corrosion Cracking of the Cover Concrete in Chloride Contaminated Reinforced Concrete Structures, *Ph.D. dissertation, Virginia Polytechnic Institute*, 1996.

[8] Spec-net, Corrosivity zones for steel construction [online] available from: http://www.spec-net.com.au/press/1014/gaa_081014/Corrosivity-Zones-for-Steel-Construction-Galvanizers-Association, 2015.

[9] J. A. Gonzales, C. Andrade, C. Alonso & S. Feliu, Comparison of Rates of General Corrosion and Maximum Pitting Penetration on Concrete Embedded Steel Reinforcement, *Cement and Concrete Research*, **25**(2), 257-264, 1995.

[10] M. S. Darmawan & M. G. Stewart, Effect of Pitting Corrosion on Capacity of Prestressing Wires, *Magazine of Concrete Research*, **59**(2), 131-139, 2007.

[11] V. Červenka, J. Cervenka, L. Jendele, *Atena Program Documentation*, Part 1-7, Červenka Consulting, Prague, Czech Republic, 2000-2013.

[12] J. Červenka and T. Sajdlová, *Most Pavla Wonky v Pardubicích*, Nelineární model nosné konstrukce - reprodukce zatěžovací zkoušky a výpočet únosnosti. (in Czech). Červenka Consulting, Prague, Czech Republic, 2016.